High-resolution study of the $K\beta_2$ x-ray spectra induced by proton and photon impact on Zr, Mo, and Pd targets

T. Ludziejewski, P. Rymuza, and Z. Sujkowski
Sołtan Institute for Nuclear Studies, 05-400 Świerk, Poland

B. Boschung, J.-Cl. Dousse, B. Galley, Z. Halabuka,* Ch. Herren, J. Hoszowska,† J. Kern, and Ch. Rhême
Physics Department, University of Fribourg, CH-1700 Fribourg, Switzerland

M. Polasik
Institute of Chemistry, Nicholas Copernicus University, 87-100 Toruń, Poland
(Received 28 December 1994)

$K\beta_2$ x-ray spectra of Zr, Mo, and Pd induced by photons and 16-, 25-, and 45-MeV protons were measured with a transmission bent crystal spectrometer. The average M-shell ionization probabilities were determined with the assumption that the yields in the $K\beta_2$ satellite region are due only to the M-shell ionization accompanying the removal of the K-shell electron. In the case of photoionization, these yields were found to exceed significantly those calculated with the sudden-approximation model for the shakeoff plus shakeup. Likewise, the corresponding yields for collisions with protons exceed those expected for the combined effect of the direct Coulomb ionization and the shake mechanism. The solid-state effects, as well as the direct knockout of the M-shell electron by the photoelectron (or the δ electron), are discussed in view of their possible effect on the line intensity in the satellite region. The direct Coulomb ionization probabilities in near central collisions with protons are determined from the difference of the relative yields of Kβ_2 satellites in the proton- and photon-induced ionization. The underlying assumption is that the shake and solid-state effects are independent of the ionizing agent and that the secondary-electron ionization is similar in the two processes. The results are compared with the semiclassical approximation calculations exploiting relativistic hydrogenic and Dirac-Hartree-Fock wave functions.

PACS number(s): 32.30.Rj, 32.70.Jz, 32.80.Fb, 34.50.Fa

I. INTRODUCTION

Measurements of x-ray spectra with a resolution comparable to the natural widths of the emission lines provide rich and valuable information about the structure of singly and multiply ionized atoms, as well as about the processes governing their production. Satellites appearing in such spectra arise as a consequence of the differences in nuclear charge screening and in angular-momentum coupling for different possible hole configurations. They are the experimental signature of multiple-inner-shell ionization.

In the case of charged-particle impact, measurements of x-ray satellites allow one to investigate the inner-shell ionization mechanisms involved in nearly central collisions. This method has been extensively explored in the past for the determination of the L-shell ionization probabilities induced by heavy-ion impact on light targets [1–15]. Many of these works have also addressed the validity of the independent-particle approximation for the description of the multiple-inner-shell ionization.

More recently the "satellite" method has been applied for heavier targets and energetic collisions [16–25]. These investigations were inspired mostly by the growing interest in a detailed knowledge of the ionization processes for which the interaction is relatively strong and for which, besides the direct Coulomb ionization, the charge exchange plays an important role [23–25].

Furthermore, it has been shown [12,19] that the method based on the observation of the K x-ray satellites can be extended to the investigation of ionization processes in shells higher than L. That technique was used for the determination of the M-shell ionization probabilities induced by He impact [19–21] and later, with the help of extensive multiconfiguration Dirac-Fock calculations, for the determination of the M-shell ionization probabilities accompanying heavy-ion bombardment [26,27]. Fast ionization processes are of particular interest here due to the increasing sensitivity of the theoretical differential cross sections to the details of the wave functions.

Satellite spectra are, however, specific not only for the charged-particle impact. They may accompany photoionization as a result of many-electron processes. Multiple vacancy states induced by photon impact can therefore provide insight into electron correlation mechanisms [28,29].

*Present address: Physics Department, University of Basel, CH-4056 Basel, Switzerland.
†On leave from the SINS, Świerk, Poland.

 ©1995 The American Physical Society

An interesting feature of the satellite spectra involving outer-shell electrons is their sensitivity to the chemical environment, that is, the chemical bonding, or the physical state of the target atom medium. The so-called "chemical effects" may influence the satellite line shapes [30–34] as well as the relative x-ray intensity ratios or diagram line profiles [35–39]. This sensitivity to the chemical or physical state of the target atom can be exploited in various applications [30,31,34].

The precise diffraction x-ray spectroscopy applied to the highly charged few-electron ions may also provide a powerful probe of our understanding of the relativistic many-body problem [40] and can be used to test the accuracy of the approximations used for the description of retardation and correlation energies [41] as well as radiative corrections [42]. These fundamental corrections can be analyzed by comparing the experimental energies and intensities of radiative transitions in multiply ionized atoms [43,44] with Hartree-Fock or Dirac-Fock calculations.

In this paper we present a detailed analysis of the $K\beta_2$ satellite spectra of Zr, Mo, and Pd targets induced in collisions with proton and photon beams of varied energies. The main goal was to provide a deeper insight into the structure of the $K\beta_2 M^1$ transitions and to determine the M-shell ionization probabilities due to direct Coulomb ionization and shakeoff plus shakeup effects. Our interest in the M-shell ionization by protons was stimulated by the recent observation of systematic discrepancies between the experimental data on the inner-shell ionization induced by ^{4}He beams and the semiclassical approximation calculations exploiting hydrogeniclike wave functions (SCA-HYD) [20,22].

In the case of the M-shell ionization by fast light particles the direct Coulomb ionization is accompanied by a non-negligible ionization resulting from multielectron (e.g., shakeoff and shakeup) processes. To estimate the relative contribution of these processes in the case of charged-particle impact, we have also measured the $K\beta_2$ line structure resulting from photoionization. Unexpectedly, we have found that the M-shell ionization probabilities determined from the photoinduced $K\beta_2 M^1$ satellite intensities exceed significantly those calculated in the framework of the sudden approximation and exhibit a nonmonotonic dependence on the target atomic number. Several possible processes leading to the $K\beta_2$ line enhancement in the satellite line region are discussed. The most likely explanation seems to be the solid-state effects.

The direct Coulomb ionization probabilities were estimated from the differences of the total p_M for proton and photon impact. The M-shell ionization probabilities are compared with the SCA calculations exploiting hydrogeniclike and self-consistent-field Dirac-Fock wave functions.

The paper is organized as follows. Section II describes the experimental method and Sec. III presents the method of the data analysis. The results are presented in Sec. IV together with the discussion of the experimental data. Finally, Sec. V gives the summary and concluding remarks.

II. EXPERIMENT

Measurements of the $K\beta_2$ line structures induced by proton beams were carried out at the Paul Scherrer Institute (PSI) in Villigen, Switzerland with the use of a DuMond type curved crystal spectrometer. For the diffraction of the x rays the (1 1 0) reflecting planes of a 1-mm-thick quartz crystal plate bent to the radius of 3.13 m were used. The spectrometer was operated in a modified DuMond slit geometry. A detailed description of the spectrometer and the experimental setup can be found elsewhere [45].

Self-supporting metallic foils of natural Zr, Mo, and Pd with thicknesses 12.7 mg/cm^2, 26.4 mg/cm^2, and 25.9 mg/cm^2, respectively, were used as targets. The proton beams of energies 16, 25, and 45 MeV were obtained from the PSI variable energy cyclotron. Beam intensities typically of 2–3 μA were monitored by 0.6-cm^3 Si(Li) detector. Targets were cooled by a low-pressure He gas flow, pumped through the target chamber. Instrumental resolution (width of the Gaussian instrumental response) was determined by measuring the 63.120 81-keV γ line in the ^{169}Yb decay in the third order of reflection. The same line provided the energy calibration of the spectrometer.

Photoionization measurements were performed with a similar spectrometer installation at the Fribourg University [46], with the use of the same diffraction crystal and geometrical conditions. The x-ray beams were provided by an x-ray tube equipped with a gold anode. Measurements were performed in two energetic modes: the low-energy regime (where the x-ray tube operated at 30–35 kV 30 mA) and the high-energy (80 kV, 30 mA) regime. The foil thicknesses were 31.7 mg/cm^2, 26.4 mg/cm^2, and 25.9 mg/cm^2 for Zr, Mo, and Pd targets, respectively. In both regimes the voltage was thus below the K-shell ionization threshold of the gold anode. Figure 1 presents a comparison of the $K\beta_2$ spectra of Zr, Mo, and Pd, induced by the 16-MeV proton beam and by the photons in the high-energy regime.

For elements with an atomic number $Z<50$ the satellite structure of the $K\beta_2$ line partially overlaps with the K-absorption edge region. In order to correct the spectra for the steplike increase of self-absorption in the target, the K-absorption edge profiles of Zr, Mo, and Pd targets were measured. In these measurements the spectrometer was used as a monochromator. The monoenergetic x rays passing through the 31.7-mg/cm^2 Zr, 54.4-mg/cm^2 Mo, and 25.9-mg/cm^2 Pd thick foils were recorded with a Ge(Li) detector. For illustration, the K-absorption edge of Mo is shown in Fig. 2.

III. METHOD OF DATA ANALYSIS

The measured $K\beta_2$ spectra were corrected to account for the self-absorption in the target of the observed x rays. For medium-heavy elements such as Zr, Mo, and Pd, these corrections are of prime importance because the K absorption edges fall in the $K\beta_2 M^1$ satellite regions. The change of the self-absorption as a function

of the photon energy was deduced for each target from the K-absorption edge measurements. For the photoinduced spectra the spectral intensity distribution of the x-ray tube was used to calculate the variation of the target activity as a function of the penetration depth of the ionizing radiation. In contrast, the proton-induced ionization was assumed to be constant over the entire thickness of the target. This assumption is reasonable since, due to the small energy loss of the protons in the targets, the K-shell ionization cross sections can be considered as nearly constant throughout the target thickness. The spectra were normalized to give equal peak heights of the $K\beta_2$ diagram line in the raw and the corrected spectra.

Independently of the type of the ionizing particle, the measured $K\beta_2$ spectra exhibit the pronounced high-energy structures (see Fig. 1). These additional lines can be classified as $K\beta_2 M^1$ satellites, which are the $K\beta_2$ ($4p_{1/2,3/2} \rightarrow 1s$) transitions in atoms with an additional M-shell hole. Assuming this identification, one can determine the average M-shell ionization probability p_M. In the independent-particle framework, the probability that the collision with the impact parameter b produces m vacancies in the K shell and n vacancies in the M shell is given by the expression

$$P_{mK,nM}(b) = \binom{2}{m}\binom{18}{n}[p_K(b)]^m \times[1-p_K(b)]^{2-m}[p_M(b)]^n[1-p_M(b)]^{18-n}, \quad (1)$$

where p_K and p_M are the K- and M-shell ionization probabilities per electron. We assume here that there are no differences in the M-subshell ionization probabilities $p_M(b)$. Alternatively, one can state that p_M represents the probability averaged over the M subshells.

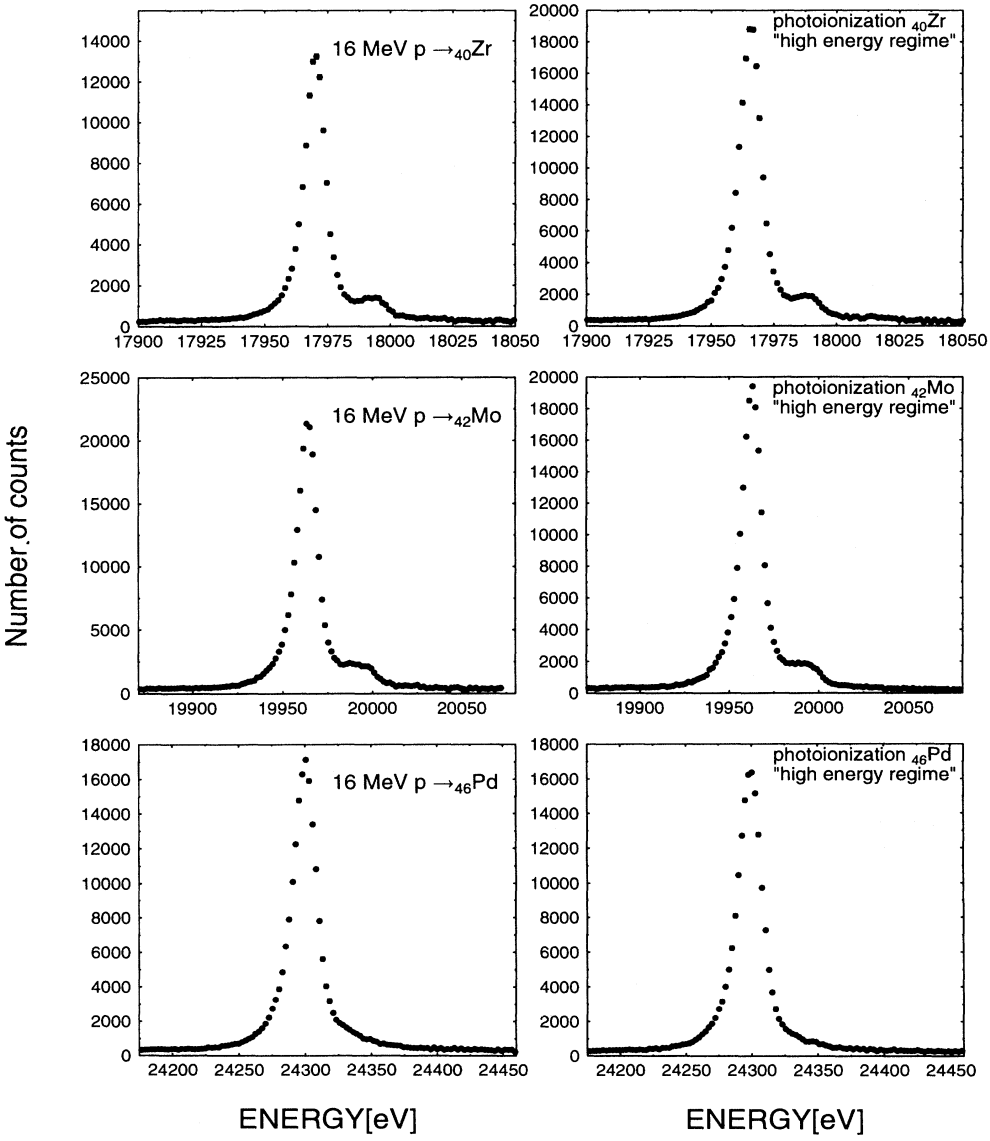

FIG. 1. Examples of the $K\beta_2$ x-ray spectra excited by 16-MeV proton impact and photons.

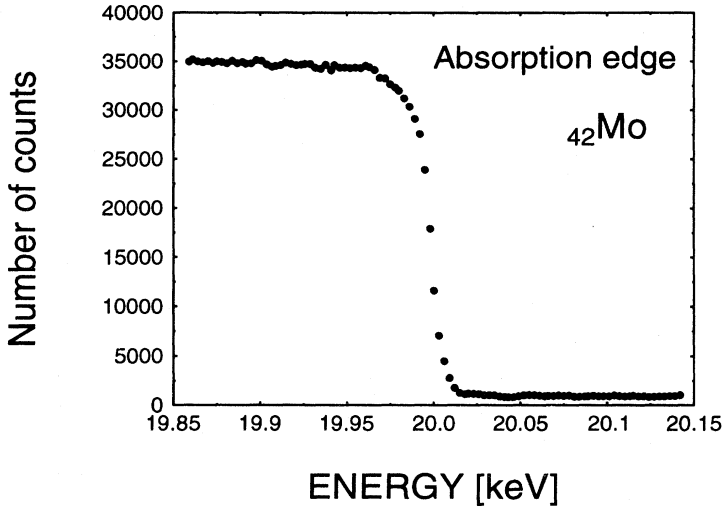

FIG. 2. K absorption edge of molybdenum measured with the spectrometer operating as a monochromator.

The corresponding cross sections are obtained by the integration over the impact parameter b

$$\sigma_{mK,nM} = 2\pi \int_0^\infty bP_{mK,nM}(b)db. \tag{2}$$

Noting that for charged particles p_M is essentially constant in the impact parameter range $(0,b_{\max})$, where the K-shell ionization occurs, one finds that

$$\frac{\sigma_{1K,1M}}{\sigma_{1K,0M}} = I_M = \frac{18p_M(0)}{1-p_M(0)} \tag{3}$$

and therefore

$$p_M^{\text{tot}}(0) = 18p_M(0) = 18\frac{I_M}{18+I_M}, \tag{4}$$

where $p_M^{\text{tot}}(0)$ is the total M-shell ionization probability. Relation (4) is independent of the way of vacancy production and holds also for the shakeoff probabilities with $p_M(0)$ replaced by p_M^{shake}.

In order to extract the information about the relative intensity I_M of the $K\beta_2$ satellite lines, the experimental $K\beta_2$ spectra were decomposed into the $K\beta_2M^0$ and $K\beta_2M^1$ components. The latter ones were constructed theoretically using the transition energies and transition probabilities determined from the extensive multiconfiguration Dirac-Fock (MCDF) calculations. The MCDF method, which is used in the present study, has been described in detail in many papers [47,48,26]. For the $K\beta_2$ transitions, these calculations should be carried out in the modified special average level (MSAL) version. Some essential ideas of the MCDF-MSAL method are given below.

Within the MCDF scheme the effective Hamiltonian for an N-electron system is expressed by

$$H = \sum_{i=1}^{N} h_D(i) + \sum_{j>i=1}^{N} C_{ij}\ , \tag{5}$$

where $h_D(i)$ is the Dirac operator for the ith electron and the terms C_{ij} account for electron-electron interactions and are based on the one-photon exchange processes, which result from the sum of the Coulomb interaction operator (due to longitudinally polarized photons) and the transverse Breit operator (due to transversely polarized photons). In the MCDF method an atomic state function with the total angular momentum J and parity p is assumed to have the multiconfigurational form

$$\Psi_s(J^p) = \sum_m c_m(s)\Phi(\gamma_m J^p), \tag{6}$$

where $\Phi(\gamma_m J^p)$ are configuration state functions (CSFs), $c_m(s)$ are the configuration mixing coefficients for the state s, and γ_m represents all information required to uniquely define a certain CSF.

There exist various versions of MCDF calculations depending on the choice of the form of the energy functional. In the standard optimal-level version of MCDF (MCDF-OL), we get for a particular state the optimal energy, the optimal set of one-electron spinors, and the optimal set of the CSF mixing coefficients $\{c_m(s)\}$. The application of the MCDF-OL version to the calculations of the transition probabilities should take into account the nonorthogonality of the spinors corresponding to the pairs of initial and final states. Moreover, in the theoretical studies on $K\alpha$ L or/and M satellite transitions, the transitions may occur between hundreds of states. The application of the MCDF-OL method for the present study would thus necessitate a separate MCDF-OL calculation for each state, which is very time consuming.

In order to cope with the above difficulties, some other methods (different from MCDF-OL) are used to calculate the transition probabilities. The main feature of those methods is the fact that they use the common set of orbitals for all the initial and final states. Two standard schemes have been elaborated up to now, which are based on this idea, namely, the average-level version of MCDF (MCDF-AL) and the extended average-level version of

MCDF (MCDF-EAL).

Preliminary test calculations have shown that MCDF-AL and MCDF-EAL schemes are indeed not accurate enough in some cases. The reason seems to be that the functional does not consider the different number of the initial and final states. Therefore the orbitals obtained in this scheme in a sense favor those states (initial or final) that are more numerous.

In the MCDF-MSAL method, which is used in this work, $E_{\rm opt}$ [47,48,26] is expressed in the form

$$E_{\rm opt} = \frac{1}{\lambda+1}\left[\frac{\lambda}{n_i}\sum_{i=1}^{n_i} H_{ii} + \frac{1}{n_f}\sum_{f=1}^{n_f} H_{ff}\right], \qquad (7)$$

where H_{ii} and H_{ff} are the diagonal contributions to the Hamiltonian matrix, the first sum runs over all the initial CSFs (n_i), the second one over all the final CSFs (n_f), and λ is a factor.

One can see that if $\lambda = 1$ we obtain a formula in which the compensation for the exaggerated contribution of the more numerous states (initial or final) to the energy functional is complete. This already results in a good reproduction of the relative positions of the spectral lines. For $\lambda = 1$, however, the calculated (diagram and satellite) line energies for transitions $K\alpha_{1,2}L^nM^r$, $K\beta_{1,3}L^nM^r$, and $K\beta_2L^nM^r$ are shifted with respect to the experimental ones by similar amounts. Test calculations have shown that the optimum values of λ depend strongly on the type of spectral line, but are almost independent of the type of an atom. The λ values can therefore be treated as parameters characteristic for the type of spectral line. It is very important that this simple formula, with particular values of $\lambda = 0.5$, 0.65, and 0.8 for $K\alpha_{1,2}L^nM^r$, $K\beta_{1,3}L^nM^r$, and $K\beta_2L^nM^r$ transitions, respectively, reproduces very well the experimental diagram and satellite lines for many medium Z atoms. The presence of λ in formula (7) enables in the simplest way the compensation of the difference of description of the initial and final states, which is the main problem in the reliable theoretical (MCDF) study of the structure of $K\alpha_{1,2}L^nM^r$, $K\beta_{1,3}L^nM^r$, and $K\beta_2L^nM^r$ lines. Therefore, formula (7) provides a simple and effective way of calculating the absolute positions of spectral lines.

This functional has already been applied with success in the extensive study of the $K\alpha_{1,2}L^nM^r$, $K\beta_{1,3}L^nM^r$, and $K\beta_2L^nM^r$ lines in Mo [26], Pd, and La [27]. For each $K\alpha_{1,2}L^nM^r$, $K\beta_{1,3}L^nM^r$, and $K\beta_2L^nM^r$ transition the MCDF-MSAL results are in an excellent agreement with the experiment [26,27]. This means that the MCDF-MSAL scheme is adequate to describe reliably the relevant states. In the present study we used the computer program package GRASP [47], which allows reliable MCDF calculations with the inclusion of Breit interaction and QED corrections. The $4d^45s^2$ and $4d^{10}$ closed valence shell ground-state configurations were assumed for Mo and Pd correspondingly, while for Zr the realistic $4d^2$ open valence shell configuration was used.

The numerical method used for the decomposition of the experimental spectra to the $K\beta_2M^0$ and $K\beta_2M^1$ components is based on the Lavenberg-Marquardt nonlinear least-squares fitting routine. Since the instrumental resolution necessary to separate these structures is comparable to the natural widths of the $K\beta_2$ lines, the theoretical line shapes were calculated by folding their Lorentzian natural shape with the Gaussian instrumental response. These so-called Voigt profiles were calculated by means of an efficient convolution method based on the fast Fourier transform algorithm. Due to the lack of precise experimental or theoretical data on the natural $K\beta_2$ linewidths for elements with $Z \leq 46$, the Lorentzian width of each component was taken to be equal to the average value of $K\alpha_1$ and $K\alpha_2$ linewidths given in the tables of Salem and Lee [49]. The theoretical $K\beta_2M^0$ and $K\beta_2M^1$ line profiles were computed by summing up all the Voigt functions (corresponding to particular initial and final states) multiplied by their transition probabilities. In the fit, the instrumental width (the full width at half maximum of the Gaussian part of the Voigt function), the overall energy shift, the linear background, and the peak heights of the $K\beta_2M^0$ and $K\beta_2M^1$ components were let free. The instrumental widths extracted from the fit were in each case in good agreement with the value given by the direct measurement with the radioactive source (see Sec. II).

In Fig. 3 we present results of the fitting routine for Zr, Mo, and Pd $K\beta_2$ spectra induced by 16-MeV protons. The solid line represents the overall theoretical line shape fitted to the spectrum corrected for absorption. The dashed lines represent the decomposition of the spectra into the $K\beta_2M^0$ and $K\beta_2M^1$ components. To visualize the role of the self-absorption corrections the uncorrected spectrum is also presented (open circles). In addition, in the upper part of each spectrum we plot schematically the results of the MCDF calculations. The solid bars depict the energies and transition probabilities of each $K\beta_2M^{0,1}$ multiplet component. The imperfect description of the low-energy tail of the $K\beta_2$ line observed in Fig. 3 can be due to the radiative Auger effect, Raman or Compton scattering of the characteristic x rays in the volume of the target or crystal, as well as to an instrumental effect. However, no asymmetry of the diffracted lines has been found in measurements of the instrumental response for the third-order reflection of the γ line of the ^{169}Yb source. It has been estimated that the errors of the absolute intensity of the diagram $K\beta_2$ line stemming from the "asymmetry effect" are for all cases not larger than 5%. Assuming that the diagram and satellite lines are affected by the similar amount, the influence of this uncertainty on the M-shell ionization probabilites is to a large extent reduced.

The relative intensities X^n ($n = 0, 1$) of the $K\beta_2M^n$ lines determined from the fit reflect the number of M-shell holes present at the moment of the K x-ray transition. For a comparison with the theoretical calculations of the ionization probabilities given by formula (4) these values have to be converted to the relative cross sections I^n (n =0,1) for producing zero and one M-shell vacancy states. This relation can be expressed as

$$X^0 = (I^0 + RI^1)\omega_{\beta_2},$$
$$X^1 = (I^1 - RI^1)\omega_{\beta_2}, \qquad (8)$$

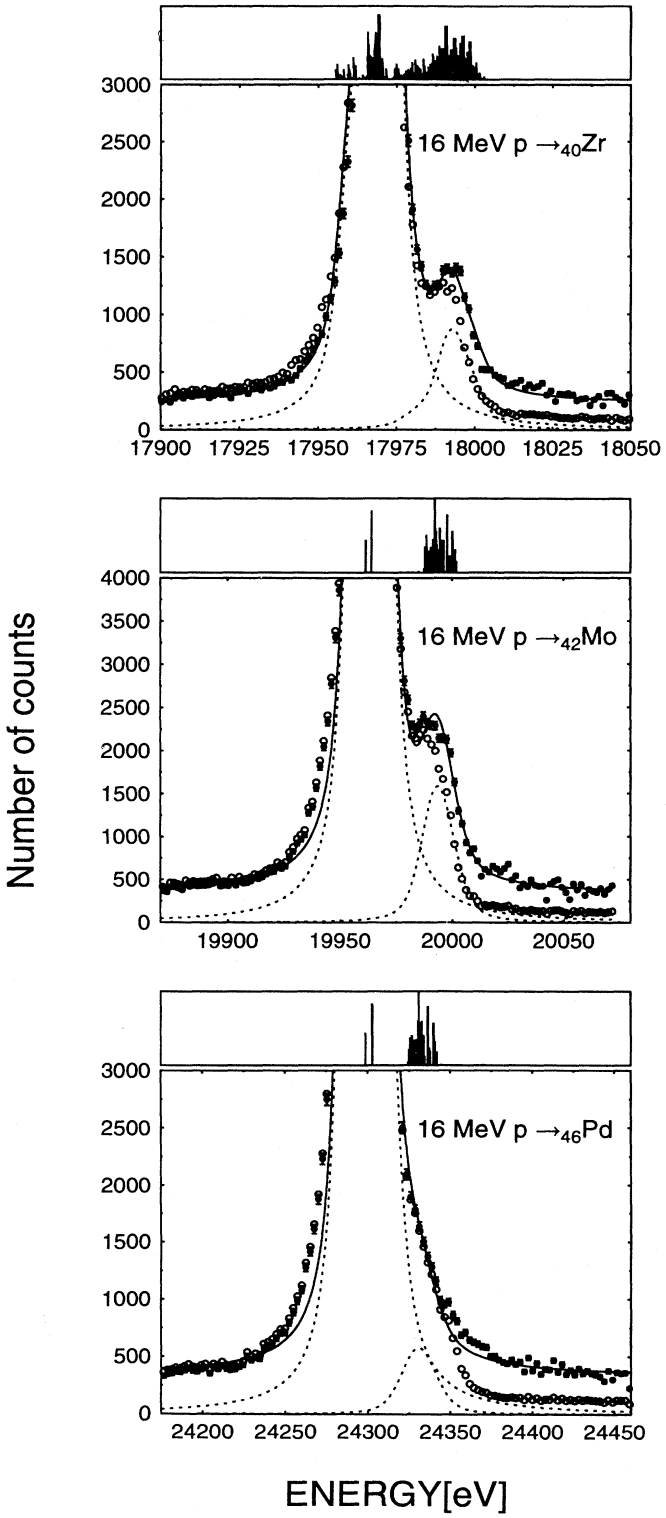

FIG. 3. Comparison between the experimental and fitted $K\beta_2$ satellite spectra for 16-MeV proton impact on Zr, Mo, and Pd targets. The solid lines represent the total fitted line profiles and the dashed lines show the decomposition of the spectra to the $K\beta_2 M^0$ and $K\beta_2 M^1$ components. The open circles mark the spectra not corrected for self-absorption. The results of MCDF calculations are presented schematically in the upper part of each spectrum.

where ω_{β_2} is the partial fluorescence yield for $K\beta_2$ transition and R is the probability that the M-shell hole is filled prior to the K x-ray emission. The rearrangement probability R (the probability that the M shell is filled prior to the radiative $K\beta_2$ transition) can be determined from the formula

$$R = \frac{\Gamma_M^A + \Gamma_M^R}{\Gamma_K + \Gamma_M}, \tag{9}$$

where Γ_K and Γ_M are the total atomic-level widths of K and M levels while Γ_M^A and Γ_M^R are the partial widths for radiative and Auger processes of the M shell.

Considering the fluorescence yields for the $K\beta_2$ transition to be independent of the number of M-shell holes and exploiting relation (8), the primary vacancy yields I_M used for the determination of p_M according to formula (4) can be expressed by

$$I_M = \frac{I^1}{I^0} = \frac{X_M}{1 - R(1 + X_M)}, \quad \text{where} \quad X_M = \frac{X^1}{X^0}. \tag{10}$$

The R values were estimated to be equal to 0.029, 0.040, and 0.053 for Zr, Mo, and Pd targets, respectively. For the M shell the partial widths for Auger Γ_M^A, Coster-Kronig Γ_M^{CK}, and radiative processes Γ_M^R were determined by interpolating the weighted theoretical values of McGuire [50,51] while the total K-shell widths were taken from tables [52].

In Eq. (9) the influence of the CK transitions is neglected since these transitions can lead only to a rearrangement of the holes within the M subshells and do not change the total number of M-shell holes created originally in the collision (the super Coster-Kronig transitions that create two M-shell holes are negligibly weak, or forbidden, for $40 \leq Z \leq 46$). Moreover, the radiative K transitions are much faster than the radiative or Auger transitions filling the M shell. Therefore, as far as the total number of M-shell holes is considered, the resulting rearrangement probabilities R are small. As a consequence, the M-shell ionization probabilities determined from the $K\beta_2 M^1$ satellites are practically unaffected by the generally large uncertainties of M-shell Auger and radiative transitions. In contrast, the partial M-level widths for the radiative and nonradiative processes constitute a significant source of errors in the conventional coincidence method.

As mentioned above, the CK transitions have only a minor influence on the total number of the M-shell holes. They can, however, significantly change the population of the M-subshell holes prior to the $K\beta_2$ x-ray emission. For example the partial widths for Zr $M1, M2, M3$ subshells are $\Gamma_{M1}^{CK} \simeq \Gamma_{M1}^{total} \simeq 6.5$ eV and $\Gamma_{M2}^{CK} \simeq \Gamma_{M2}^{total} \simeq \Gamma_{M3}^{total} \simeq 2.4$ eV [50], while the total K-shell width is $\Gamma_K^{total} \simeq 3.8$ eV [52]. This implies that approximately one-half of the holes originally created in the $3s$, and $3p_{1/2,3/2}$ states $(M1, M2, M3)$ subshells are transferred to the $3d_{3/2,5/2}$ $(M4, M5)$ states. According to the detailed discussion of Polasik [48] and later Carlen *et al.* [26,27], the average energy shift of $K\alpha$ as well as $K\beta_{1,3}$ transitions with additional $3s$ or $3p$ holes is larger than that with additional $3d$ holes. This implies that the the-

oretically constructed spectrum may differ in the overall shape from the experimental one, due to these Coster-Kronig rearrangement processes. In view of the practical difficulties (more than 14 000 components to be considered in the case of $K\beta_2$ satellite structure of Zr) these effects have not been taken into account in the present study. One could expect, however, that the error introduced by this approximation is small in the case of $K\beta_2$ transitions for the following reasons: (i) the good separation of the $K\beta_2 M^1$ satellite structure and (ii) the "inner" character of the spectator holes, implying that the relative energy splitting of states with $3s$ or $3p$, and $3d$ holes is smaller in the case of the $K\beta_2$ than, e.g., of the $K\beta_{1,3}$ transitions, where the radiative transition involves the shell in which the additional holes have been created.

IV. RESULTS AND DISCUSSION

Following the procedure described in details above, we have calculated the average M-shell ionization probabilities due to the proton and photon impact. The results are collected in Tables I and II. The listed errors are due only to the fit procedure and do not include the systematic errors due to the assumed line-shape model or the self-absorption corrections.

Within the processes responsible for the multiple K- plus M-shell vacancy production all except the direct Coulomb ionization are common for both photoionization and charged-particle impact. Therefore, we focus first on the discussion of the M-shell ionization probabilities accompanying the K-shell photoionization.

A. M-shell ionization accompanying K-shell photoionization

In the case of photoionization the decisive role in K- plus M-shell hole production is played by multielectron processes. These processes, which are possible due only to the residual electron-electron interaction, are divided in our discussion into three parts: (1) the "shake" processes, discussed here in terms of the sudden approximation; (2) the direct knockout of an M-shell electron by a photoelectron; and (3) the reminding part of the electron correlation that is not included in Secs. IV A 1 and IV A 2.

TABLE I. Experimental M-shell ionization probabilities deduced from the $K\beta_2 M^1$ satellites of Zr, Mo, and Pd induced by photoionization. The heading "low E" means the low-energy regime, while "high E" means the high-energy regime. (For details see the text.)

Atom	Photoionization low E	Photoionization high E
Zr	7.58 ± 0.38	8.39 ± 0.35
Mo	8.20 ± 0.38	8.60 ± 0.36
Pd	2.15 ± 0.26	2.46 ± 0.24

TABLE II. Same as Table I but for collisions with 16-, 25-, and 45-MeV protons.

Atom	16-MeV p	25-MeV p	45-MeV p
Zr	9.25± 0.62	9.16 ± 0.67	9.76 ± 0.55
Mo	9.45± 0.36	8.52 ± 0.46	8.10 ± 0.41
Pd	4.12± 0.30	3.17 ± 0.33	3.10 ± 0.34

1. Shake processes

The excitation of passive electrons, which fail to relax completely during the rapid change of the central potential associated with the emission of a photoelectron (or a δ electron, or β particle), is often called the shake process. The sudden collapse of an atomic wave function can either excite electrons to unoccupied valence states (shakeup) or eject them to the continuum (shakeoff). For energies of photons well above the double ionization threshold, the shakeoff and shakeup processes accompanying photoionization are conveniently discussed in terms of the sudden approximation (SA). In the SA framework, the probability for a change of the electron configuration is calculated under the assumption that the change of the potential is instantaneous.

Following the expression of Carlson *et al.* [53], the probability of promoting an electron from the state described by the quantum numbers n, l and containing N electrons to a higher unoccupied shell or continuum is given by

$$P_{nl} = 1 - \left(\left| \int \Psi'^{*}_{nl} \Psi_{nl} \right|^2 \right)^N - P_F, \tag{11}$$

where P_F is the contribution of the transitions to the x filled states forbidden by the Pauli exclusion principle and is expressed by

$$P_F = \sum_{n'=1}^{x} \frac{NN'}{2(2l+1)} \left| \int \Psi'^{*}_{n'l} \Psi_{nl} \right|^2 . \tag{12}$$

The ionization probability due to the shake processes can therefore be determined in terms of the simple overlap integrals of the wave functions representing the initial and final states.

According to [54], the sudden approximation is valid when the energy of the ejected electron $E_{\rm ph}$ exceeds significantly the ionization threshold $E_{\rm bind}$ for the shakeoff electron. Indeed, a comparison of the experimental data generally yields fair agreement with the SA theory as long as the process is sufficiently violent and involves electrons from different shells. Carlson *at al.* found for photoionization [55] and electron impact ionization [56] that the shake probability is in good agreement with the SA calculations when $E_{\rm ph} > 3E_{\rm bind}$. A similar criterion for K- and L-shell shakeoff processes was found theoretically by Sachenko *et al.* [57].

The photoionization was induced in the present work by the photons with continuous energy spectra emitted by the x-ray tube. To test the applicability of the SA

theory for these data, the average photoelectron energies $E_{\rm ph}$ were determined from the measured energy distribution of photons. In the calculations the incident photon energy distribution was weighted by the relative cross sections for the K-shell photoionization. The resulting average photoelectron energies were found to be 9.0 keV for Zr, 9.3 keV for Mo, and 9.6 keV for Pd in the high-energy regime and 3.3 keV, 2.9 keV, and 3.0 keV correspondingly, for the low-energy regime. The average binding energies of M-shell electrons are $E_{\rm bind}$ =0.264 keV for Zr, $E_{\rm bind}$ =0.315 keV for Mo, and $E_{\rm bind}$ =0.442 keV for Pd. Therefore, as long as the average photoelectron energies are considered, the application of the SA model seems to be well justified in our case.

A number of different calculations of the shakeoff and shakeup probabilities in the SA limit were reported in the literature. Starting from the work of Carlson and Krause, these calculations utilize rather realistic Hartree-Fock or Hartree-Fock-Slater wave functions [53–56]. Most of these calculations were performed for noble gases and only rarely for elements with open valence shells. To establish a better base for our discussion we decided to recheck the interpolated values of Carlson *et al.* [53]. Our calculations follow the SA model defined by formulas (11) and (12) and use the self-consistent Dirac-Fock wave functions from the MCDF code GRASP [47]. The resulting M-shell shake probabilities due to the $1s$ hole production for Zr, Mo, and Pd are listed in Table III. For comparison the results of Carlson *et al.* are also presented. It can be seen that present calculations are in fair agreement with the former results.

Figure 4 shows the comparison between the SA calculations and the experimental p_M values obtained with two different average energies of incident photons. The measured data are systematically larger than the SA calculations. Only for Pd can an almost satisfactory agreement be seen. Furthermore, the theory predicts a monotonic decrease of the shakeoff probability with Z,

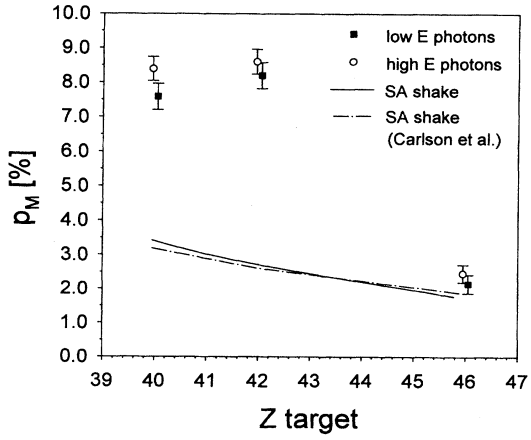

FIG. 4. Total M-shell ionization probabilities versus target atomic number for two different average photon energies. Solid line, our results of the sudden-approximation calculations of the shake probabilities; dash-dotted line, interpolated values taken from [53].

TABLE III. Theoretical M-shell ionization probabilities due to the shake processes calculated in the sudden-approximation limit.

Atom	$P_M^{\rm shake}$ (%) Ref. [58]	$P_M^{\rm shake}$ (%) This work
Zr	3.192	3.428
Mo	2.620	2.730
Pd	1.867	1.831

while the experimental p_M is the largest for Mo, where $p_{\rm exp}/p^{\rm SA}_{\rm theor}\simeq 3.0$. In addition, the measurements show systematically larger p_M for the higher average energy of the photon beam. The excess of the experimental p_M over the SA calculations for Zr and Mo is in disagreement with our expectations since, due to the underlying assumption of the sudden change of potential, the SA results should be regarded rather as an upper limit of the shakeoff probability.

2. *Direct photoelectron–M-shell electron collision*

When an electron is emitted from the atomic core, there is a possibility for that outgoing electron to collide with other target electrons. Such direct electron-electron collisions (DCs) may result in an additional ionization. The relative importance of this process with respect to the shakeoff was first discussed by Feinberg [58] for the case of β decay. His considerations are to some extent related to our problem, since the β electron emerges from the center of the atom, while the K-shell photoelectron emerges nearly from the center. The originally quoted estimate $p_K^{\rm DC}/p_K^{\rm shake} \approx \frac{B_K}{E_\beta}$ (E_β denotes the energy of the β particle, while B_K is the binding energy) suggests that the dominant contribution to the K-shell ionization in β decay comes from the shakeoff effect, while the DC mechanism is a small correction. More refined theoretical studies [59] confirmed that the DC contribution to p_K is not significant even in the favorable cases of β emitters.

For the M-shell ionization of Zr, Mo, and Pd by photons the approximate relation of Feinberg gives a relative contribution of the direct knockout that is not larger than 15%, but its applicability in this case is questionable: first, because of the different energy distribution of β particles and photoelectrons, and second, due to the different structure of the wave functions of the K- and M-shell electrons. In our case, the estimation of relative contribution of the M-shell shake and DC processes is further complicated by the fact that the energy distribution of photoelectrons is not monoenergetic. Thus, for the low-energy part of the continuous photon spectra the assumptions of the sudden approximation may not hold true. In this case, the shake probabilities can be noticeably smaller than those calculated in the SA limit, while simultaneously the contribution of the DC mechanism can be significantly enhanced. It appeared recently (see, e.g., [29]) that for photoelectrons with $E_{\rm ph}$ close to the ionization potential the relative contribution of the

outer shell electron knockout can be as high as 20–40 %.

On the basis of the estimates mentioned we cannot precisely determine the contribution of the DC by the photoelectron to the total M-shell hole production. We can, however, state that the direct knockout mechanism cannot fully explain the large discrepancies between the SA calculations and the experimental p_M. More likely, the DC process, as well as the breakdown of the sudden approximation for low photon energies, is responsible for the observed inequality of p_M for the two different $E_{\rm ph}$ distributions.

3. Electron correlation

Under the term of correlation process in ionization we understand the phenomena that involve at least two directly interacting electrons. Therefore, DC as well as shakeoff belong to this category, although, the shake processes can be well described by the one-electron sudden-approximation model. As it has been pointed out by Amusia [29], the correlational effects are the strongest for the cases when the energy of the direct electron-electron interaction is larger than the total energy of each of the interacting electrons. This situation is easily achievable for outer atomic shells, for electrons from the same shell, or for the near-threshold phenomena. A good illustration of this statement is the increasing importance of the direct knockout at small photoelectron energies.

Besides the shake and DC processes there are other correlation effects such as the configuration interaction that may influence the generalized shake amplitudes. Evidence of the latter process can be found in the double K-shell photoionization. While in general non-negligible, the correlation that is not included in the SA shake theory and DC process plays no role in the case of the K- plus M-shell ionization by energetic photons or protons.

B. M-shell ionization accompanying proton impact

The measured M-shell ionization probabilities versus the energy of the incident protons are plotted in Fig. 5. One can see a similar dependence of the p_M on the target atomic number as that observed for the photoionization. In particular, the experiment yields similar p_M for Zr and Mo, while for Pd the experimental p_M is substantially smaller. For a given Z the experimental p_M decreases as a function of the projectile velocity.

As we pointed out already before, the direct Coulomb ionization (DCI) contributes significantly to the total p_M for charged-particle impact. Although attempts to calculate the DCI in a full quantum-mechanical formalism were reported in the literature, the data on the inner-shell ionization probabilities are conveniently discussed in terms of the SCA. The SCA based on the first-order perturbation theory is especially appropriate for the description of the impact-parameter-dependent single-electron ionization probability for fast and asymmetric ion-atom collisions. Recent studies [20,21] of the L- and M-shell ionization probabilities in collisions with energetic He

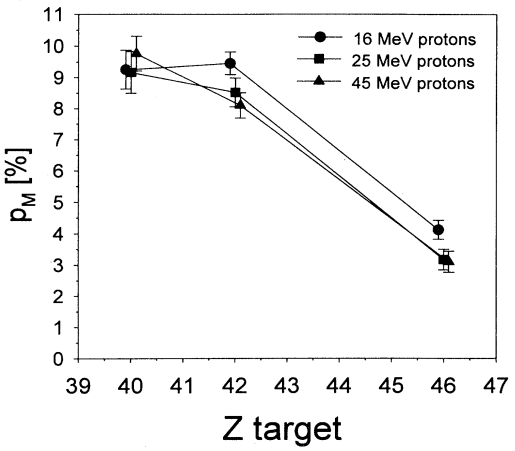

FIG. 5. Same as in Fig. 4 for collisions with 16-, 25-, and 45-MeV protons.

particles showed, however, systematic discrepancies between experimental data and the SCA version of Trautmann and Rösel [60,61]. The disagreement between SCA calculations exploiting relativistic hydrogeniclike wave functions and the classical hyperbolic trajectories was found to grow rapidly with reduced velocity, being particularly high in the case of the M-shell ionization. Similar discrepancies have been also observed in the case of L- and M-shell ionization by heavy ions [18,25–27].

Recently, an improved version of the SCA program was developed [62], where the single-electron ionization probabilities are calculated with the use of relativistic Hartree-Fock (SCF) wave functions instead of hydrogeniclike ones. The modification leads to a much better agreement between experiment and theory for light and heavy ions showing the importance of realistic wave functions in the SCA calculations for "fast" ion-atom collisions.

In Figs. 6(a)–6(c) we have plotted a comparison of the experimental total p_M for proton impact on Zr, Mo, and Pd with the SCA-SCF calculations of the DCI process and SA calculations of the shake probability. The SCA calculations were performed for an impact parameter b=500 fm, which, according to the relation $\bar{b} = \int b^2 p_K(b) db / \int b p_K(b) db$, gives the maximum contribution to the K-shell ionization cross section. One can see again that the experimental p_M significantly exceeds the sum of the theoretical shake and DCI contributions for Zr and Mo, while a fair agreement is obtained for Pd. The energy dependence of p_M in each case seems to be rather well reproduced by the theory.

For 16-MeV protons on Zr, Mo, and Pd systems the SCA-HYD calculations of the average δ-electron energies yield 13 keV, 17 keV, and 30 keV and are correspondingly larger for larger impact energies. Therefore, the SA is valid for estimation of the shakeoff + shakeup contributions to the total p_M. Assuming that the contribution of other than DCI processes is the same for proton and photon impact, the DCI M-shell ionization probability is given as a difference of the total p_M for these two cases. In Fig. 7 the direct Coulomb M-shell ionization prob-

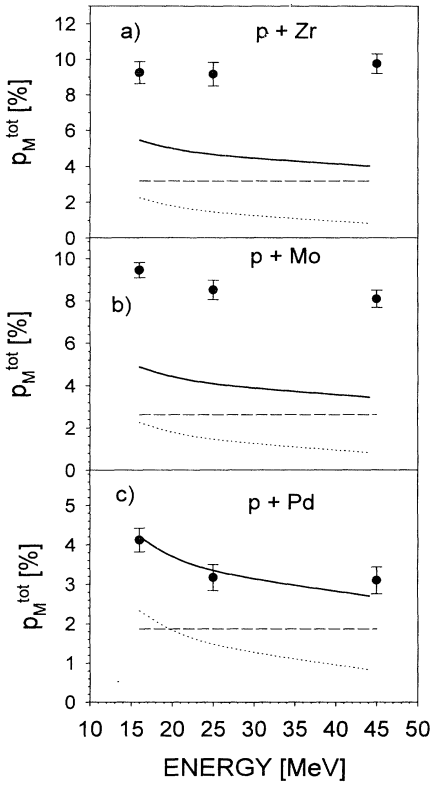

FIG. 6. Comparison of the experimental and theoretical M-shell ionization probabilities for (a) Zr, (b) Mo, and (c) Pd targets bombarded by the 16-, 25-, and 45-MeV protons with the SA calculations of the shake probabilities (dash line) SCA-SCF calculations of the direct Coulomb ionization by protons (dotted line), and the sum of DCI and shake contributions (solid line).

abilities due to the proton impact are shown together with the predictions of SCA-HYD and SCA-SCF calculations. In the SCA-HYD calculations, to account for screening effects, the effective nuclear charge according to the Slater recipe was used. The effect of the recoil of the target nucleus was taken into account.

Both SCA calculations predict the M-shell ionization probabilities to be almost independent of the atomic target number and show a very similar dependence on the projectile energy. The large differences between the SCA-HYD and SCA-SCF calculations in the case of M-shell ionization of Zr, Mo, and Pd by 16-, 25-, and 45-MeV protons illustrate the importance of using realistic wave functions in the theoretical description of fast ionization processes. For completeness we present in Fig. 7 the data for which the low- and high-energy results on photoionization were used. Considering the large uncertainties stemming from the experimental errors, as well as the approximate procedure used, one can state that the overall dependence of the experimental direct Coulomb ionization probabilities is well reproduced by the SCA calculations. Unfortunately, the large experimental errors do not allow a critical comparison between SCA calculations exploiting hydrogenic and self-consistent field wave functions.

The applicability of the method used for the extraction of the direct Coulomb ionization probabilities is in fact independent of to what extent the SA is fulfilled and how important the DC process is as long as the energy distributions of δ electrons and photoelectrons are the same. This condition, however, is not satisfied in our case, since the δ-electron energies are generally larger than the corresponding photoelectron energies. The systematic error of the procedure (and therefore of the experimental data depicted in Fig. 7) depends on the detailed balance between the electron knockout and shakeoff plus shakeup processes, particularly for the low-energy tail of the ejected electrons, where the application of the SA is questionable.

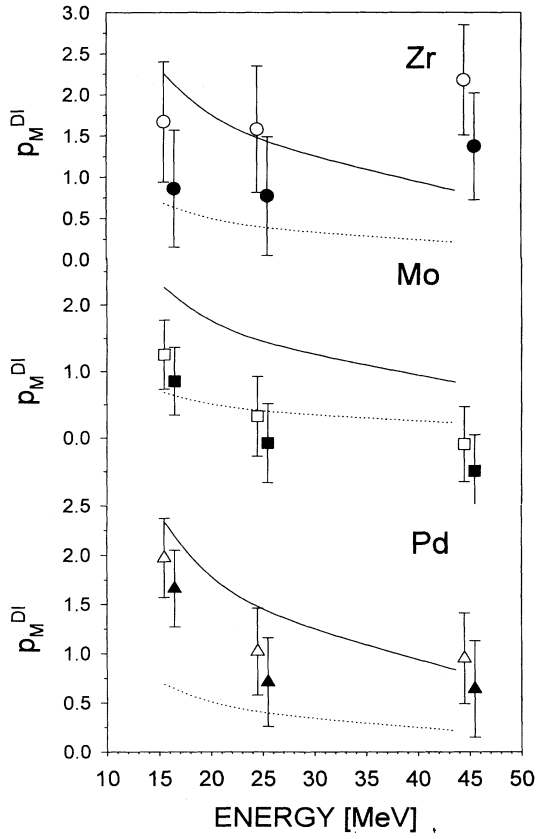

FIG. 7. Direct Coulomb ionization probabilities for 16-, 25-, and 45-MeV protons on Zr, Mo, and Pd, systems compared with the SCA-SCF and SCA-HYD calculations. The experimental ionization probabilities were evaluated under the assumption that the contribution of shake and direct knockout is given by the photoionization data in the high-energy limit (full markers) and low-energy limit (empty markers).

C. Solid-state effects

It is well known that the emission of x rays is sensitive to the chemical environment. For the satellite transitions, variation of their intensity with the chemical state of the target medium arises from the fast interatomic electron transfer or differences in rearrangement probabilities [30–32]. For example, it has been found [30] for the third row elements, where the valence electrons belong to the M shell, that the crossover or rearrangement transitions in chemical compounds can compete with $K\alpha$ x-ray emission leading to a substantial reduction of the $K\alpha$ satellites. Variations of the relative intensity distributions of L x-ray satellites have been found for various Mo alloys [34]. The influence of environment in the case of $K\beta_2$ transitions for elements of the fourth row is much less important due to relatively faster radiative $K\beta_2$ transitions. Moreover, the fast rearrangement processes can lead only to the reduction of the observed $K\beta_2$ satellites.

For transitions in singly ionized atoms, it has been found that the intensity ratios of transitions involving inner and outer shells depend on the local density of valence electrons in the host material [31,35,36,39,33]. For example, it has been shown for molybdenum [35] that the $L_{\gamma 1}/L_{\beta 1}$ ($4d_{3/2} \rightarrow 2p_{1/2}$ to $3d_{3/2} \rightarrow 2p_{1/2}$) intensity ratio increases with the valence occupation density, i.e., with the ionicity of the compound. Transitions involving outer shells are obviously much more influenced by the chemical environment than transitions between inner shells.

Similar effects of the environmental dependence of valence-to-core transitions can be responsible for the observed line enhancement in the $K\beta_2$ satellite line region. The ground-state configurations of atomic Zr, Mo, and Pd are [Sr]$4d^2$ [Kr]$4d^5 5s^1$ and [Kr]$4d^{10}$, which implies that, due to selection rules, the most intense transitions from the N shell are the $K\beta_2$ ones (i.e., transitions from $4p_{1/2,3/2}$ to $1s$ states). The forbidden quadrupole $K\beta_4$ ($4d_{3/2,5/2} \rightarrow 1s$) transitions have for medium-heavy atoms very low intensities [e.g., $I(K\beta_4)/I(K\beta_2) \sim 1.1 \times 10^{-3}$ for Mo].

For metallic targets, however, there is a possibility that these transitions occur from the strongly delocalized $4d$ states that for Zr, Mo, and Pd belong to the conduction band. In this case, transitions of the valence electrons can acquire the dipole character bringing a sharp increase of intensity. Effects of the strong intensity enhancement for the quadrupole $K\beta_5$ ($3d_{3/2,5/2} \rightarrow 1s$) transitions have been observed for atoms $21 < Z < 29$ where the $3d$ subshells belong to the valence band [15].

In the case of Zr, Mo, and Pd the energies of the $K\beta_4$ transitions are very close to those of the $K\beta_2 M^1$ satellites. For example, the MCDF calculations for isolated atoms yield for the $K\beta_4$ transitions 18 002.7 eV (Zr), 20 004.2 eV (Mo), and 24 327.3 eV (Pd), while the average energies of $K\beta_2 M^1$ satellite lines are 18 001.1 eV, 19 997.7 eV, and 24 332.8 eV for Zr, Mo, and Pd, respectively. Therefore, within the instrumental resolution, valence to K-shell transitions match the energies of the $K\beta_2 M^1$ satellites.

There are two additional indications that suggest that the $K\beta_4$ transitions may influence the observed line intensity in the Zr, Mo, and Pd satellite region.

(i) The theoretical profiles of the $K\beta_2 M^1$ satellite lines calculated on the basis of extensive MCDF calculations describe rather poorly the experimental line profile in the satellite region. However, as mentioned before, these effects can be connected with the rearrangement processes.

(ii) The observed discrepancies between experimental p_M and theoretical predictions depend nonmonotonically on Z. One can expect that the effect of valence to K-shell transition is the most significant for the half-filled valence shell [15]. For the $4d$ subshells this condition is fulfilled for Mo, for which the ratio of the experimental to theoretical p_M is the largest.

The importance of the $K\beta_4$ transitions can be clarified in experiments where the $K\beta_2$ satellite line shapes and intensities are investigated for various chemical states of the target [63].

V. SUMMARY AND CONCLUSIONS

High-resolution measurements have been performed for the Zr, Mo, and Pd $K\beta_2$ lines produced by proton and photon beams of different energies. The observed satellite structures were analyzed by fitting the theoretical line profiles constructed on the basis of extensive MCDF calculations. Assuming that the $K\beta_2$ satellite lines originate from the K- plus M-shell ionization, the average M-shell ionization probabilities were determined for proton and photon impact.

The photon data demonstrate an essential excess of the satellite line yields over those calculated within the sudden approximation with the use of reliable SCF wave functions. We would expect the SA theory to overestimate the experimental p_M since the assumed condition of a sudden change of the central potential is not fulfilled for the low-energy part of the ejected photoelectron spectrum. In addition, it was found that the M-shell ionization probabilities increase with the average energy of the photon beam. Two processes leading to the observed energy dependence are discussed; the direct knockout of M-shell electrons by photoelectron and the breakdown of the sudden approximation for the low-energy photoelectrons and δ electrons. The resulting p_M depend most likely on the interplay of both processes.

The results for protons show essentially the same behavior of the total p_M as in the case of photoionization. Even if the direct Coulomb ionization is taken into account, the experimental p_M are systematically larger than the sum of direct ionization and shakeoff contributions.

By combining the results for proton impact with those for photons we determined the experimental direct Coulomb ionization probabilities in near central collisions. The overall dependence of the experimental p_M is rather well reproduced by the SCA theory. In view

of the rather large systematic and statistical errors, the procedure does not allow for a critical discussion of the dependence of the SCA calculations on the wave functions used.

Finally, it is suggested that the observed enhancement of the satellite lines for both proton and photon impact is due to the contribution of the $K\beta_4$ ($4d_{3/2,5/2} \rightarrow 1s$) radiative transitions. For metals with $40<Z<48$, where the $4d_{3/2,5/2}$ states belong to the valence band, the quadrupole $K\beta_4$ transition can acquire dipole properties, which results in a strong enhancement of its intensity.

ACKNOWLEDGMENTS

The authors acknowledge the assistance of Dr. P.A. Schmelzbach and other members of the PSI Phillips Cyclotron staff for providing us with the excellent proton beams. One of us (T.L.) wants to express particular thanks for the kind hospitality during his stay at Fribourg University. Partial support for this work was provided by the Polish Committee for Scientific Research (KBN) Grants Nos. 2P 302 119 07 and 2 2322 92 03 and by the Swiss National Science Foundation.

[1] P. Richard, I.L. Morgan, T. Furuta, and D. Burch, Phys. Rev. Lett. **23**, 1009 (1969).
[2] D. Burch, P. Richard, and R.L. Blake, Phys. Rev. Lett. **26**, 1355 (1971).
[3] A.R. Knudson, D.J. Nagel, P.G. Burkhalter, and K.L. Dunning, Phys. Rev. Lett. **26**, 1149 (1971).
[4] D.G. McCrary, M. Senglaub, and P. Richard, Phys. Rev. A **6**, 263 (1972).
[5] C.F. Moore, M. Senglaub, B. Johnson, and P. Richard, Phys. Lett. **40A**, 107 (1972).
[6] P.G. Burkhalter, A.R. Knudson, D.J. Nagel, and K.L. Dunning, Phys. Rev. A **6**, 2093 (1972).
[7] C.F. Moore, D.K. Olsen, B. Hodge, and P. Richard, Z. Phys. **257**, 288 (1972).
[8] T.K. Li, R.L. Watson, and J.S. Hansen, Phys. Rev. A **8**, 1258 (1973).
[9] R.L. Kauffman, J.H. McGuire, and P. Richard, Phys. Rev. A **8**, 1233 (1973).
[10] F. Hopkins, D.O. Elliot, C.P. Bhalla, and P. Richard, Phys. Rev. A **8**, 2952 (1973).
[11] R.L. Watson, F.E. Jenson, and T. Chiao, Phys. Rev. A **10**, 1230 (1974).
[12] K.W. Hill, B.L. Doyle, S.M. Shafroth, D.H. Madison, and R.D. Deslattes, Phys. Rev. A **13**, 1334 (1976).
[13] *Atomic Inner Shell Processes*, edited by B. Crasemann (Academic, New York, 1975), Vols. I and II.
[14] *Atomic Physics: Accelerators*, edited by P. Richard (Academic, New York, 1980).
[15] B.K. Agarwal, in *X-Ray Spectroscopy*, edited by D.L. MacAdam, Springer Series in Optical Sciences Vol. 15 (Springer-Verlag, Berlin, 1979).
[16] B. Perny, J.-Cl. Dousse, M. Gasser, J. Kern, Ch. Rhême, P. Rymuza, and Z. Sujkowski, Phys. Rev. A **36**, 2120 (1987).
[17] R. Salziger, G.L. Borchert, D. Gotta, O.W.B. Schult, D.H. Jakubassa-Amundsen, P.A. Amundsen, and K. Rashid, J. Phys. B **22**, 821 (1989).
[18] D.F. Anagnostopoulos, G.L. Borchert, and D. Gotta, J. Phys. B **25**, 2771 (1992).
[19] M. Carlen, J.-Cl. Dousse, M. Gasser, J. Kern, Ch. Rhême, P. Rymuza, Z. Sujkowski, and D. Trautmann, Europhys. Lett. **13**, 231 (1990).
[20] P. Rymuza, T. Ludziejewski, Z. Sujkowski, M. Carlen, J.-Cl. Dousse, M. Gasser, J. Kern, and Ch. Rhême, Z. Phys. D **23**, 81 (1992).
[21] M. Carlen, J.-Cl. Dousse, M. Gasser, J. Hoszowska, J. Kern, Ch. Rhême, P. Rymuza, and Z. Sujkowski, Z. Phys. D **23**, 71 (1992).
[22] B. Boschung, M.W. Carlen, J.-Cl. Dousse, B. Galley, Z. Halabuka, Ch. Herren, J. Hoszowska, J. Kern, Ch. Rhême, T. Ludziejewski, M. Polasik, P. Rymuza, and Z. Sujkowski, *PSI Annual Report* No. 147, 1993 (unpublished), and unpublished.
[23] P. Rymuza, Z. Sujkowski, M. Carlen, J.-Cl. Dousse, M. Gasser, J. Kern, B. Perny, and Ch. Rhême, Z. Phys. D **14**, 37 (1989).
[24] D.F. Anagnostopoulos, G.L. Borchert, D. Gotta, and K. Raschid, Z. Phys. D **18**, 139 (1991).
[25] T. Ludziejewski, P. Rymuza, Z. Sujkowski, D. Anagnostopoulos, G. Borchert, M. Carlen, J.-Cl. Dousse, J. Hoszowska, J. Kern, and Ch. Rhême, Acta Phys. Pol. B **25**, 699 (1994).
[26] M.W. Carlen, M. Polasik, B. Boschung, J.-Cl. Dousse, M. Gasser, Z. Halabuka, J. Hoszowska, J. Kern, B. Perny, Ch. Rhême, P. Rymuza, and Z. Sujkowski, Phys. Rev. A **46**, 3893 (1992).
[27] M.W. Carlen, B. Boschung, J.-Cl. Dousse, Z. Halabuka, J. Hoszowska, J. Kern, Ch. Rhême, M. Polasik, P. Rymuza, and Z. Sujkowski, Phys. Rev. A **49**, 2524 (1994).
[28] U. Becker, in *X-Ray and Inner-Shell Processes*, edited by Manfred Krause and Thomas Carlson, AIP Conf. Proc. No. 215 (AIP, New York, 1990), p. 621.
[29] M.Y. Amusia, in *X-Ray and Inner-Shell Processes* (Ref. [28]), p. 25.
[30] R.L. Watson, J.A. Damarest, A. Langenberg, F.E. Jenson, J.R. White, and C.C. Bahr, IEEE Trans. Nucl. Sci. **NS-26**, 1352 (1979).
[31] S. Raman and C.R. Vane, Nucl. Instrum. Methods B **3**, 71 (1984).
[32] C.R. Vane, L.D. Hulett, S. Kahane, F.D. McDaniel, W.T. Milner, G.D. O'Kelley, S. Raman, T.M. Rosseel, G.G. Slaughter, S.L. Varghese, and J.P. Young, Nucl. Instrum Methods Phys. Res. Sect. B **3**, 88 (1984).
[33] J. Kawai, Nucl. Instrum. Methods Phys. Res. Sect. B **75**, 3 (1993).
[34] T.M. Rosseel, J.P. Young, J.M. Dale, A. Das Gupta, L.D. Hullet, H.F. Krause, C.T. Liu, S. Raman, and C.R. Vane, J. Phys. F **14**, 37 (1984).
[35] J. Iihara, C. Izawa, T. Omori, and K. Yoshihara, Nucl. Instrum. Methods Phys. Res. Sect. A **299**, 394 (1990).
[36] J. Iihara, T. Omori, K. Yoshihara, and K. Ishii, Nucl. Instrum. Methods Phys. Res. Sect. B **75**, 32 (1993).
[37] E. Uda, J. Kawai, and M. Uda, Nucl. Instrum Methods Phys. Res. Sect. B **75**, 24 (1993).

[38] M. Mogi, A. Ota, S. Ebihara, M. Tachibana, and M. Uda, Nucl. Instrum Methods Phys. Res. Sect. B **75**, 20 (1993).
[39] E. Hartmann, J. Phys. B **20**, 475 (1987).
[40] J. Sapirstein, Nucl. Instrum Methods Phys. Res. Sect. B **43**, 338 (1989).
[41] O. Gorceix, P. Indelicato, and J.P. Desclaux, J. Phys. B **20**, 639 (1987).
[42] P. Indelicato, O. Gorceix, and J.P. Desclaux, J. Phys. B **20**, 651 (1987).
[43] M.H. Chen and B. Crasemann, Phys. Rev. A **25**, 391 (1982).
[44] K. Schreckenbach and H.G. Börner, Phys. Lett. **63A**, 330 (1977).
[45] B. Perny, J.-Cl. Dousse, M. Gasser, J. Kern, R. Lanners, Ch. Rhême, and W. Schwitz, Nucl. Instrum. Methods Phys. Res. Sect. A **267**, 120 (1988).
[46] J. Hoszowska, J.-Cl. Dousse, and Ch. Rheme, Phys. Rev. A **50**, 123 (1994).
[47] K.G. Dyall, I.P. Grant, C.T. Johnson, F.A. Parpia, and E.P. Plummer, Comput. Phys. Commun. **55**, 425 (1989).
[48] M. Polasik, Phys. Rev. A **40**, 4361 (1989).
[49] S.I. Salem and P.L. Lee, At. Nucl. Data Tables **18**, 233 (1976).
[50] E.J. McGuire, Phys. Rev. A **5**, 1043 (1972).
[51] E.J. McGuire, Phys. Rev. A **5**, 1052 (1972).
[52] M.O. Krause and J.H. Olivier, J. Phys. Chem. Ref. Data **8**, 329 (1979).
[53] T.A. Carlson, C.W. Nestor, T.C. Tucker, and F.B. Malik, Phys. Rev. **169**, 27 (1968).
[54] T. Mukoyama and K. Taniguchi, Phys. Rev. A **36**, 693 (1987).
[55] T.A. Carlson and C.W. Nestor, Phys. Rev. A **8**, 2887 (1973).
[56] T.A. Carlson, W.E. Moddemann, and M.O. Krause, Phys. Rev. A **1**, 1406 (1970).
[57] V.P. Sachenko and E.V. Burtsev, Bull. Acad. Sci. USSR Phys. Ser. **31**, 980 (1968).
[58] E.L. Feinberg, Yad. Fiz. **1**, 612 (1965) [Sov. J. Nucl. Phys. **1**, 438 (1965)].
[59] R.L. Intermann, Phys. Rev. A **27**, 27 (1983).
[60] D. Trautmann and F. Rösel, Nucl. Instrum. Methods **169**, 259 (1980).
[61] D. Trautmann, F. Rösel, and G. Baur, Nucl. Instrum. Methods **214**, 21 (1983).
[62] Z. Halabuka, W. Perger, and D. Trautmann, Z. Phys. D **29**, 151 (1994).
[63] J. Hoszowska *et al.* (unpublished).